Numerical Investigation of Free-Surface Signatures Generated by Submerged Objects

Qiang Zhu[1], Yuming Liu[2], and Dick K.P. Yue[2]
[1]Dept of Structural Engineering, UCSD
[2]Dept of Mechanical Engineering, MIT

Abstract
We review our studies of free-surface wave patterns generated by underwater objects in the context of potential flow assumptions. Two numerical approaches for the time-domain simulation of nonlinear wave-body interactions are applied: a high-order spectral (HOS) method and a hybrid method. HOS is developed based on the perturbation theory and the use of the pseudo-spectral approach for the treatment of nonlinear free-surface boundary conditions. It accounts for nonlinear wave-wave and wave-body interactions up to an arbitrary order in the wave steepness, and achieves an exponential convergence of the solution with respect to the order of nonlinearity and the number of unknowns for moderately steep waves. Significantly, it enables an efficient simulation of nonlinear wave-body interactions and high-resolution description of free-surface features. It is, on the other hand, restricted to smooth closed bodies (such as ellipsoids). The hybrid method extends HOS by combining it with a boundary-element approach so that it is applicable to bodies with arbitrary geometries and vortex shedding. Three numerical examples, a forward moving ellipsoid in incoming waves, an underwater foil in unsteady motion, and a moored near-surface buoy in surface waves, are presented with the focus on the characteristics of the generated wave patterns.

1. Introduction

Recent development in remote sensing technology suggests a novel paradigm to detect underwater objects based on the characteristics of wave patterns of submerged bodies which may be extracted from the scanned free surface. The biological inspiration of this comes from the fishing bat (*Noctilio leporinus*). Using echolocation, the fishing bat hunts for fish swimming near the water surface by detecting ripples on water surface left by these fish.

To detect and identify underwater objects by analyzing their free-surface signatures, it is essential to understand the correlation between the generated surface wave patterns and the basic characteristics of the objects in question, e.g., size, geometry, submergence, and motion.

Numerical simulation provides a convenient and versatile mean to accurately predict the interaction between free-surface waves and submerged bodies. It requires a numerical model capable of computing with high resolution the nonlinear free-surface waves generated by a submerged body both in near and far fields. To this end, we employ the high-order spectral (HOS) method. HOS employs a perturbation analysis via a recursive algorithm to account for free-surface nonlinearity up to an arbitrary order in wave steepness. By using a pseudo-spectral treatment of the nonlinear free surface boundary conditions, HOS enables high-resolution representation of the free surface evolution. In

this approach, the computational error declines exponentially with respect to N, the number of unknowns, while with Fast-Fourier Transformation (FFT) the computational effort is proportional to $N\log N$. Owing to these valuable features, the HOS method has been successfully applied to problems where the accurate solution of nonlinear free-surface effects is essential, including nonlinear wave-wave interactions (Dommermuth & Yue, 1987), nonlinear wave-body interactions (Liu, Dommermuth & Yue, 1992), and nonlinear wave instability (Zhu, Liu & Yue 2003). In this paper, the key procedure of HOS for nonlinear wave-body interactions is outlined.

We point out that in its original formulation, HOS is only valid for problems involving closed body geometry and no vorticity shedding from the body. To overcome this, we develop a hybrid method that combines the spectral approach for high-resolution representation of free-surface waves and a boundary-element method for the treatment of arbitrary body geometry and vortex shedding (Zhu, Liu & Yue 2006). The fully-coupled interactions among the body (such as a foil), the shed vortex in the wake, and surface waves are considered. The wakes, originated from sharp trailing edges on the body, are modeled as shear layers, or, equivalently, normal dipole distributions on thin sheets. The linear free-surface effects are accounted for by utilizing a highly efficient spectral algorithm. Like HOS, this method achieves exponential convergence with respect to the number of free-surface modes and requires a (approximately) linear computational cost with the number of unknowns. We note that although nonlinear free surface effects can be considered as in HOS, at this stage, only linear effect is accounted for in the hybrid method.

Applying the HOS method and the hybrid method, in this paper, we study the generation of free-surface waves by three different near-surface objects: a spheroid moving forward in head sea; a buoy tethered by highly-extensible cable; and a foil undergoing translation and oscillation. For each case, simulations are conducted to illustrate the free-surface signatures at various conditions.

2. Mathematical formulations

We consider the problem of three-dimensional nonlinear wave-body interactions in deep water. The body is submerged below the free surface. The body may undergo forced steady and/or unsteady motions and freely respond to the action of ambient surface waves. The fluid, bounded by the free surface and the body surface, is assumed to be inviscid and incompressible, and the flow is irrotational. A space-fixed Cartesian coordinate system (x,y,z) is employed with the origin placed on the mean free surface, x and y the horizontal coordinates, and z positive pointing upward.

We define a velocity potential $\Phi(\boldsymbol{x},z,t)$ in the fluid domain, where $\boldsymbol{x}\equiv(x,y)$ is the horizontal coordinate. At any time t, Φ satisfies Laplace equation in the fluid domain and the kinematic and dynamic boundary conditions at the free surface S_f located at $z=\zeta(\boldsymbol{x},t)$. The free-surface boundary conditions can be written in Zakharov's form (Zakharov, 1968):

$$\left.\begin{aligned}&\zeta_t + \nabla_x\zeta\cdot\nabla_x\Phi^s - (1+\nabla_x\zeta\cdot\nabla_x\zeta)\Phi^s_z = 0,\\ &\Phi^s_t + g\zeta + \frac{1}{2}\nabla_x\Phi^s\cdot\nabla_x\Phi^s - \frac{1}{2}(1+\nabla_x\zeta\cdot\nabla_x\zeta)\left(\Phi^s_z\right)^2 = 0,\end{aligned}\right\} \tag{1}$$

where $\Phi^s(\boldsymbol{x},t) \equiv \Phi(\boldsymbol{x},\zeta(\boldsymbol{x},t),t)$ is the free-surface potential, $\nabla_x \equiv (\partial/\partial x, \partial/\partial y)$, and g the gravitational acceleration.

On the body surface S_b, the no-flux condition is satisfied

$$\boldsymbol{n}\cdot\nabla\Phi = \boldsymbol{n}\cdot\boldsymbol{V}_b(\boldsymbol{x},z,t), \tag{2}$$

where $\boldsymbol{n}$ is the unit normal vector which points into the fluid and $\boldsymbol{V}_b$ is the velocity of the body at the point in question. At any location on the body surface with sharp trailing edges, the Kutta condition is imposed so that the flow leaves these edges smoothly. In deep water, the fluid velocity vanishes, $\nabla\Phi \to 0$ as $z \to -\infty$. For computations, a doubly periodic boundary conditions on the horizontal plane can be specified so that the problem is periodic in both x and y.

3. Numerical methods

3.1 High-order spectral method

Perturbation expansion

In HOS, we consider the wave-body interaction problem with small wave steepness ($kA = \varepsilon << 1$, where k is the wavenumber and A is the wave amplitude) and expand the potential Φ in a perturbation series up to order M in ε:

$$\Phi = \sum_{m=1}^{M}\Phi^{(m)}, \tag{3}$$

where the superscript (m) denotes a quantity in $O(\varepsilon^m)$. We further expand the potential evaluated on the instantaneous free-surface $z = \zeta$ into a Taylor series about the mean free surface $z = 0$. Collecting terms at each order we obtain a sequence of Dirichlet conditions:

$$\Phi^{(1)} = \Phi^S \text{ and } \Phi^{(m)} = -\sum_{l=1}^{m-1}\frac{\zeta^l}{l!}\frac{\partial^l}{\partial z^l}\Phi^{(m-l)}, \text{ (for } m>1). \tag{4}$$

Correspondingly, on the instantaneous body surface $S_b(t)$, by expanding the no-flux condition (2) we have a sequence of Neumann conditions:

$$\Phi^{(1)}_n = V_{bn}(t) \text{ and } \Phi^{(m)}_n = 0, \text{ (for } m>1). \tag{5}$$

At each order m, the linearized boundary-value problem (BVP) for $\Phi^{(m)}$ includes Laplace equation $\nabla\Phi^{(m)} = 0$ inside the fluid flow, the Dirichlet condition (4) on the mean free surface, the Neumann condition (5) on the body surface, and the deep water condition $\left|\nabla\Phi^{(m)}\right| \to 0$ as $z \to -\infty$.

Spectral solution of the linearized BVP

To solve the BVP for $\Phi^{(m)}$ we distribute dipoles $\mu^{(m)}$ on the mean free surface and sources $\sigma^{(m)}$ on the instantaneous body surface S_b. In the spectral approach, we write $\mu^{(m)}$ in a double Fourier series (in *x* and *y*) and $\sigma^{(m)}$ in a Chebyshev-Fourier series (Liu, Dommermuth & Yue 1992; Zhu *et al* 1999). The perturbed potential $\Phi^{(m)}$ is then expressed as

$$\Phi^{(m)}(\mathbf{x}, z, t) = \sum_p \sum_q \mu_{pq}^{(m)}(t)\Psi_{Fpq}(\mathbf{x}, z) + \sum_k \sum_l \sigma_{kl}^{(m)}\Psi_{Bkl}(\mathbf{x}, z), \tag{6}$$

where $\mu_{pq}^{(m)}$ and $\sigma_{kl}^{(m)}$ are the (unknown) dipole and source modal amplitudes, respectively, and Ψ_{Fpq} and Ψ_{Bkl} are the free-surface/body basis functions. The exact forms of Ψ_{Fpq} and Ψ_{Bkl} are provided in Zhu *et al*. (1999). Substituting (6) into the boundary conditions (4) and (5), we can determine the modal amplitudes $\mu_{pq}^{(m)}$ and $\sigma_{kl}^{(m)}$, and subsequently, $\Phi^{(m)}$ from (6). The total velocity potential Φ is obtained by solving the BVP up to a prescribed order *M*, and summarizing $\Phi^{(m)}$.

Time integration

At each time step *t*, the free-surface potential Φ^s is known. Using HOS described above we obtain the velocity potential Φ anywhere in the flow, as well as the vertical velocity at the free surface $\Phi_z(\mathbf{x}, \zeta, t)$. A fourth-order Runge-Kutta scheme can be employed to integrate the evolution equation (1) to update Φ^s and ζ at new time.

3.2 Hybrid method

Following Zhu *et al*. (2002) and Zhu, Liu & Yue (2006), we decompose the body-wake-surface interaction into three coupled boundary-value problems. We write the total potential Φ as a linear superposition of three parts, $\Phi = \phi_b + \phi_w + \phi_f$, where ϕ_b represents the contribution from the body, ϕ_w the contribution from the vorticity wake, and ϕ_f the influence of the free surface. For the body influence problem for ϕ_b, we assume that ϕ_w and ϕ_f are given, and apply the no-flux boundary condition (2) to determine ϕ_b. Similarly, we formulate the free-surface problem for ϕ_f as a Dirichlet problem by specifying the value of ϕ_f at the mean free surface (with $\phi_f = \Phi - \phi_b - \phi_w$). Finally, we model ϕ_w as the induced velocity potential of zero-thickness shear layers. These layers originate from the sharp trailing edges of the body. At each instant, the strength of the newly created potion of the layer is determined by the Kutta condition at the trailing edge, provided that ϕ_b and ϕ_f are known. The rest of the layer is allowed to be advected downstream by the combined velocity field of ϕ_b, ϕ_f, and ϕ_w.

Boundary-value problem for ϕ_b

At any time *t*, if ϕ_w and ϕ_f are given, ϕ_b is determined by implementing the boundary condition (2), which is rewritten as

$$\boldsymbol{n}\cdot\nabla\phi_b = \boldsymbol{n}\cdot(\boldsymbol{V}_b(\boldsymbol{x},z,t) - \nabla\phi_w - \nabla\phi_f)\,. \tag{7}$$

Upon invoking Green's theorem, we have

$$2\pi\phi_b(\boldsymbol{r},t) + \iint_{S_b}\phi_b(\boldsymbol{r}',t)\boldsymbol{n}\cdot\nabla G(|\boldsymbol{r}-\boldsymbol{r}'|)ds' = \iint_{S_b} G(|\boldsymbol{r}-\boldsymbol{r}'|)\boldsymbol{n}\cdot\nabla\phi_b(\boldsymbol{r}',t)ds'\,, \tag{8}$$

for any $\boldsymbol{r}=(x,y,z)$ on the foil surface ($\boldsymbol{r}\in S_b$), where G is a doubly-periodic Green function (see Newman 1992).

We solve the boundary-value problem for ϕ_b by a constant panel method, in which the body surface S_b is discretized into N_b quadrilateral panels, S_{bj}, $j=1,...,N_b$. Over each panel, the body potential ϕ_b and its normal derivative (or, equivalently, the dipole strength μ_b and the source strength σ_b) are assumed to be constant. After applying (8) at the centroid of each panel, we obtain a linear system of N_b equations for N_b unknowns

$$\sum_{k=1}^{N_b} C_{jk}\mu_{bk} = \sum_{k=1}^{N_b} B_{jk}\sigma_{bk}\,, \qquad j=1,...,N_b\,, \tag{9}$$

where μ_{bk} and σ_{bk} are the values of μ_b and σ_b on panel S_{bk}, and

$$B_{jk} = \iint_{S_{bk}} G(\boldsymbol{r}_j-\boldsymbol{r}')ds'\,, \quad C_{jk} = \iint_{S_{bk}} \boldsymbol{n}\cdot\nabla G(\boldsymbol{r}_j-\boldsymbol{r}')ds'\,, \tag{10}$$

where $\boldsymbol{r}_j$ is the centroid of S_{bj}. The source strength σ_{bk} in (9) is known and is given by the boundary condition. After (9) is solved for the unknown dipole strength, the body influence potential ϕ_b and the associated velocity anywhere in the fluid are obtained.

Boundary-value problem for ϕ_f

The free-surface influence potential ϕ_f is determined from a Dirichlet boundary-value problem with its value on the mean free surface specified. At any time *t*, the total potential on the mean free surface $\Phi(x,y,0,t)$ and the free surface elevation $\zeta(x,y,t)$ are determined from time integration of the evolution equation (1). With ϕ_b and ϕ_w known, we have the Dirichlet condition on the mean free surface for ϕ_f:

$$\phi_f(\boldsymbol{r},t) = \Phi(\boldsymbol{r},t) - \phi_b(\boldsymbol{r},t) - \phi_w(\boldsymbol{r},t), \quad \boldsymbol{r}\in\bar{S}_f\,. \tag{11}$$

The spectral method described in section 3.1 is employed to solve (11) for the free-surface influence potential ϕ_f.

Determination of ϕ_w

The wake shed from the trailing edges of the body is modeled as infinitely thin shear layers, and is mathematically represented by a distribution of dipoles on the wake sheets. The instantaneous strength of the newly formed wake is determined by the Kutta condition, which specifies that the strength of dipole shedding at the trailing edge μ_w equals to the difference of body influence potential ϕ_b between the upper and lower surfaces near this edge divided by 4π. Once produced, the wake is carried downstream

by the fluid velocity and its strength is kept unchangeable due to the absence of dissipation. At any point $\boldsymbol{r}$ within the flow, the wake induced potential is given by

$$\phi_w(\boldsymbol{r},t) = \iint_{S_w} \mu_w \boldsymbol{n}' \cdot \nabla G(\boldsymbol{r} - \boldsymbol{r}') d\boldsymbol{r}', \tag{12}$$

where s_w is the instantaneous position of the wake sheet. The associated velocity field can be obtained by taking spatial derivative of (12).

Time integration

The coupled boundary-value problems for ϕ_b, ϕ_w and ϕ_f need in principal to be solved simultaneously which usually requires an expensive iteration procedure. In this study, we employ a simple approximate method to decouple the problem in the time domain. At each time step, while solving the (Neumann) boundary-value problem for ϕ_b, ϕ_w and ϕ_f are considered to be known with their values given by those at the previous time step. The same approach is applied for the determination of ϕ_w and ϕ_f. This simplification introduces an $O(\Delta t)$ error but is shown to provide a satisfactory convergence with respect to time step for practical applications (Zhu, Liu & Yue 2006).

4. Results

4.1 Free-surface signature of a submerged spheroid

We first study the wave pattern above a spheroid (which is close in geometry to a submarine). As shown in Fig. 1, the spheroid has a half length of $a=L/2$, and a half width of $b=c$. The submergence, defined as the distance from the center of the spheroid to the mean free surface, is h. The spheroid is placed in a head sea with forward speed U, and the incident wave has wave length λ, wavenumber $k = 2\pi/\lambda$, and amplitude A. The steepness of the incident wave is kA.

In this case, the free-surface signature is composed of three contributions: the incident wave; the steady Kelvin waves associated with the steady forward motion of the body consisting of the transverse and diverging wave systems; and the unsteady wave pattern generated by the diffraction of the incident wave. The characteristics of the free surface pattern is thus determined by the forward speed, the body size, as well as the incident wave parameters. Some typical wave patterns are displayed in Fig. 2. We see that as the length of the body is large compared with the incoming waves ($\lambda = L/4$) (Fig. 2a and 2b) , the radiated waves are confined with an envelope whose size is comparable with the body length. Through

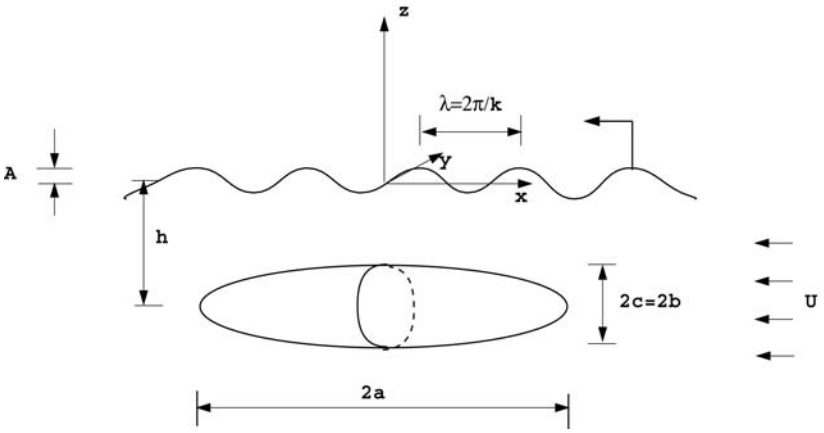

Fig. 1. Sketch of a submerged spheroid in waves.

asymptotic analysis, it has been illustrated that this envelope follows a solitary shape (Mei & Naciri, 1991). The angle between the envelope and the forward speed U decreases as U increases. With large forward speed, a narrow 'V'-shape feature is created (Fig. 2b). This phenomenon, on the other hand, becomes less pronounced as the body size is reduced (Fig. 2c and 2d).

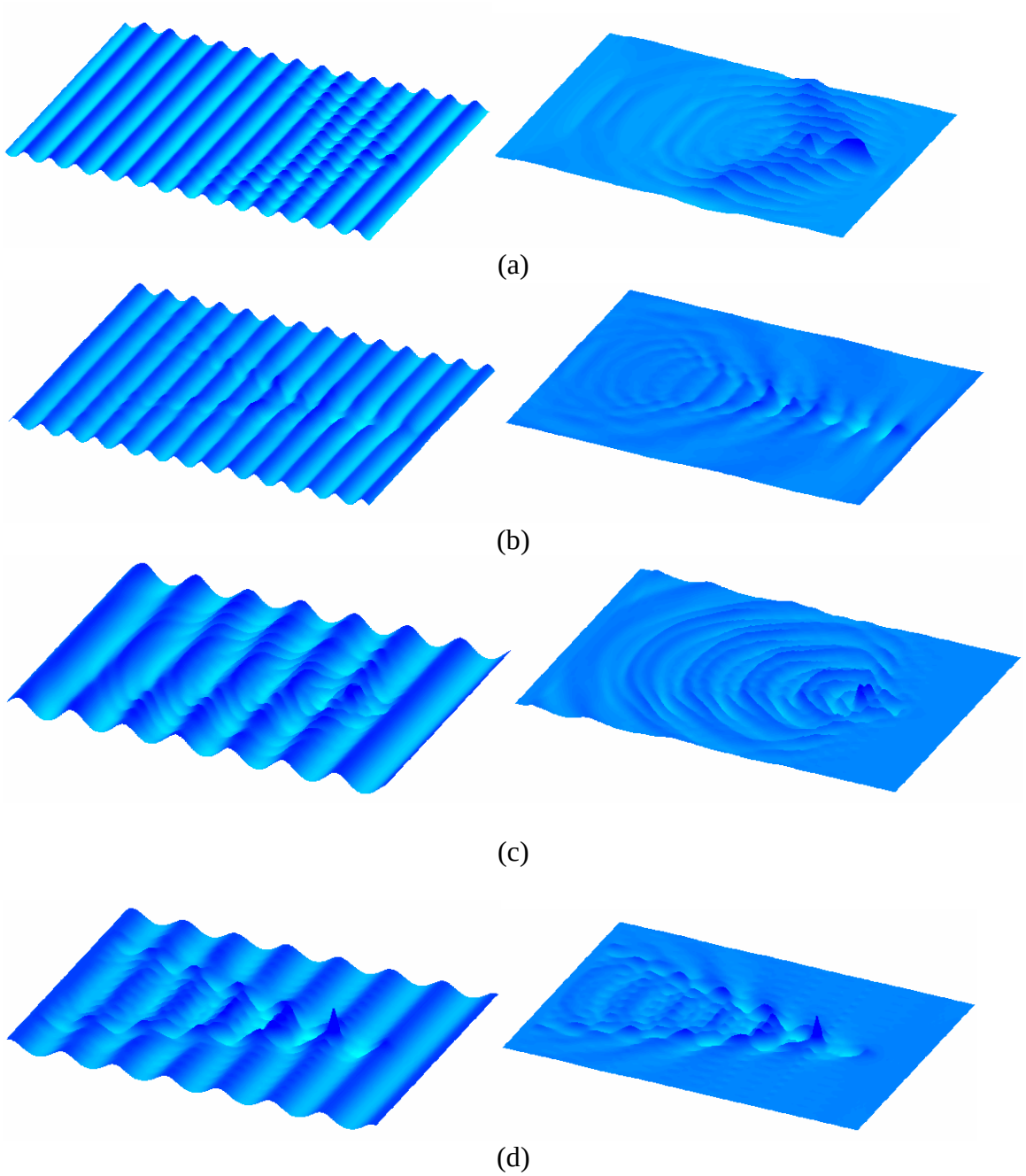

Fig. 2. Free-surface signature above a near-surface spheroid in an ambient wave field. The four cases are (a) Froude number $F_r = U/\sqrt{gL} = 0.05$, incident wave length $\lambda = L/4$ (large body, moderate speed); (b) $F_r = 0.20$, $\lambda = L/4$ (large body, large speed); (c) $F_r = 0.10$, $\lambda = 2L$ (small body, small speed); (d) $F_r = 0.20$, $\lambda = 2L$ (small

body, large speed). The wave fields shown are with (left) or without (right) incident wave components. Other parameters are: aspect ratio = c/a = 1/10, central submergence h = 1.25 c, incident wave steepness = 0.15.

4.2 Wave pattern generated by an oscillating foil

Next we consider the wave pattern generated by a submerged foil undergoing translation and unsteady oscillations. The chord length of the foil is c, the span is s. Two types of foil and motion configurations are considered. The first one is a heaving motion of a horizontal foil. The second problem we consider is the swaying motion of a foil with its span perpendicular to the free surface. The amplitude of these oscillations are A. The more detailed description of this problem and (the results) can be found in Zhu, Liu & Yue (2006).

Like the spheroid case, the free-surface signature of a translating and heaving foil also contains three components: the steady Kelvin wave pattern; the unsteady wave pattern generated by the oscillatory motion; and the waves generated by vortices in the wake.

In the heaving foil case, the solution has a strong dependence on the unsteady parameter $\tau \equiv U\omega / g$, with large free-surface response observed near the critical value $\tau = \tau_c \equiv 0.25$. Fig. 3 shows combined features of the free surface due to forward speed and oscillation of the foil for different values of τ, plotted with and without the Kelvin wake component. At the subcritical value of $\tau = 0.10$ (Fig. 3a), the unsteady wave pattern appears much weaker than the Kelvin pattern. At the critical value τ =0.25 (Fig. 3b), the wave field is dominated by the unsteady waves, demonstrating a distinctive pattern different from the Kelvin wake. At the supercritical value of $\tau = 0.50$, the unsteady waves become less pronounced and the Kelvin-like wave field reappears (Fig. 3c). In addition, a sequence of ring-shaped ripples on the track due to the underlying vortex wake is shown. The shed wake, which has initially a periodic vorticity strength, evolves under self induction into a characteristic meandering sheet with vorticity concentrated near the peaks and troughs. Eventually, the sheet curls up and evolves into a sequence of individual counter-rotating vortices. When the mean hydrodynamic force on the foil is a thrust, the wake takes the form of the reverse Kármán vortex street, in which the vortices near the peaks of the sheet are counter-clockwise, while those near the troughs are clockwise. When the foil experiences (mean) drag force, the wake resembles the classical Kármán street in which the rotational directions of the vortices are reversed. In both cases, the wake contains two arrays of vortices, one of them close to the free surface and the other far below. When the vortices in the upper row approach the free surface, they induce the characteristic sequence of ring-like wave features observed in Figure 3c. The distance between two neighboring rings is determine by the Strouhal number S_t, and is expressed as $2A/S_t = 2\pi c F_r^2 / \tau$. Based on this estimation, this distance in Figure 3a, b, and c is, 40c, 16c, and 8c, respectively. It is clear that the vortex-induced features in Figure 3a are out of the computational domain.

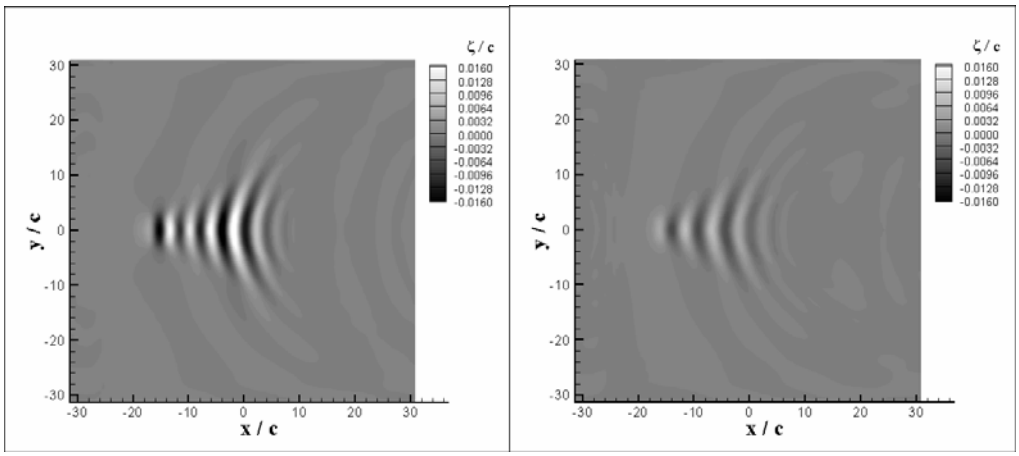

(a)

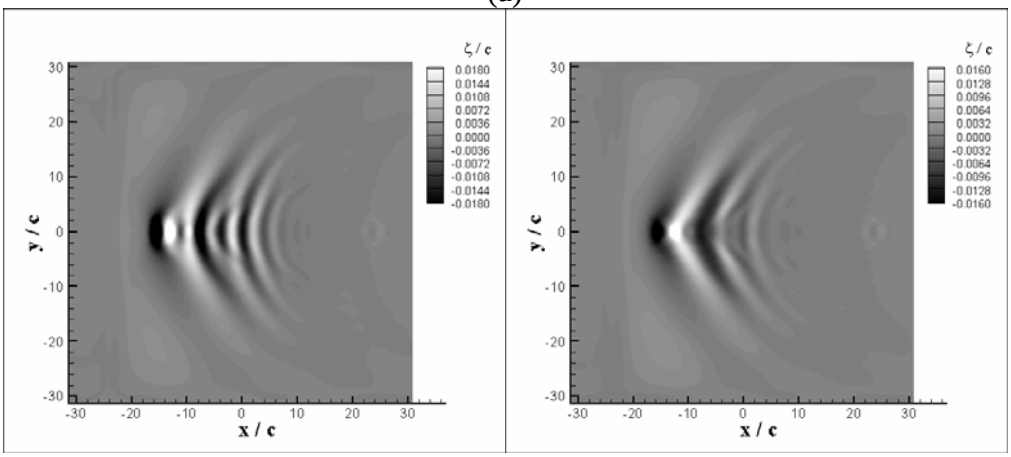

(b)

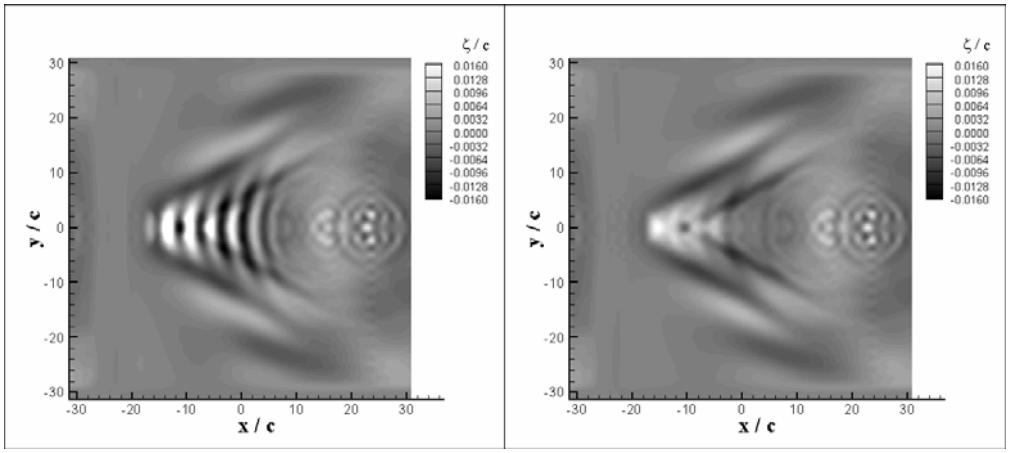

(c)

Fig. 3. Free-surface waves generated by the heaving motion of a horizontal foil with aspect ratio $s/c = 5, F_r = 0.80, h/c = 1.5$, and $A/c = 0.2$ at (a) $\tau = 0.10$; (b) $\tau = 0.25$; and (c) $\tau = 0.50$. The submergence h is defined to be the distance from the mean free surface to the mean position of the center of the foil. The wave fields shown are with (left) and without (right) steady Kelvin wake components.

Unlike the horizontal foil case, the problem of a vertical foil in sway motion is much less sensitive to τ. As shown in Fig.4, the unsteady waves are non-symmetrical with respect to the track of the foil. As τ increases, the wavenumber and amplitude of the unsteady waves increase accordingly, while the abrupt rise of the amplitude of the unsteady waves in the region near $\tau = \tau_c$ is not observed. The vortex-induced waves appear as well and generally become stronger with larger values of τ. These vortex-induced waves appear on ring-like shapes. Their locations correspond to the position of the underlying vortices in a Kármán (or reverse Kármán) vortex street and are therefore away from the centerline and exhibit the characteristic meandering pattern of the vortex street. The distance between two neighboring rings in the *x* direction is estimated to be $A/S_t = \pi c F_r^2 / \tau$, which is estimated to be 20*c*, 8*c*, and 4*c* for the cases in Figure 74, b, and c, respectively.

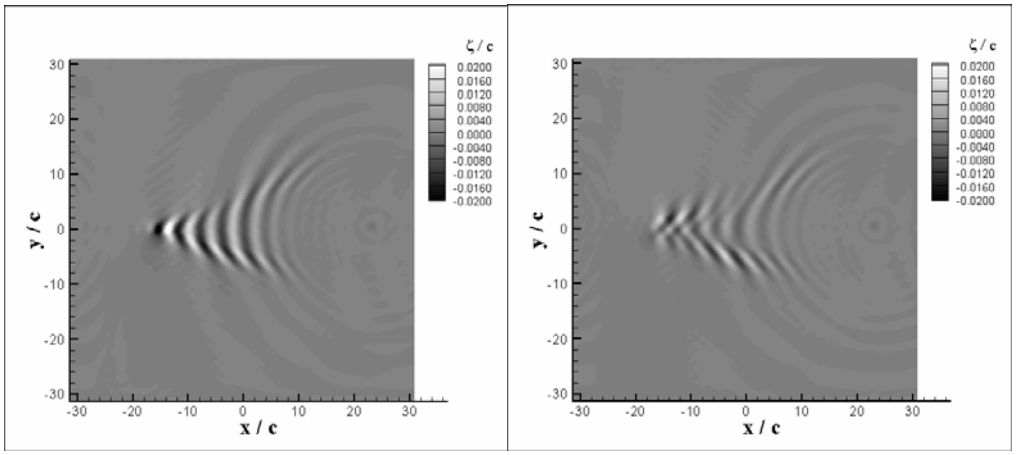

(a)

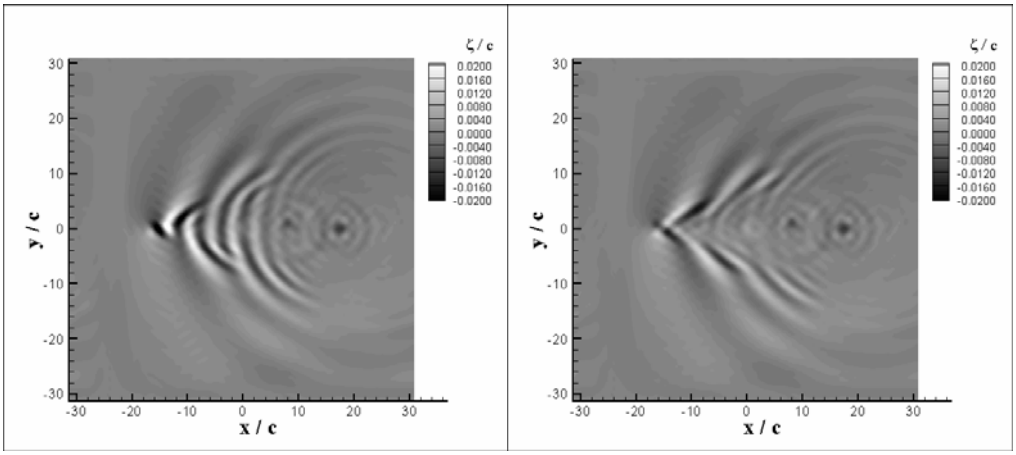

(b)

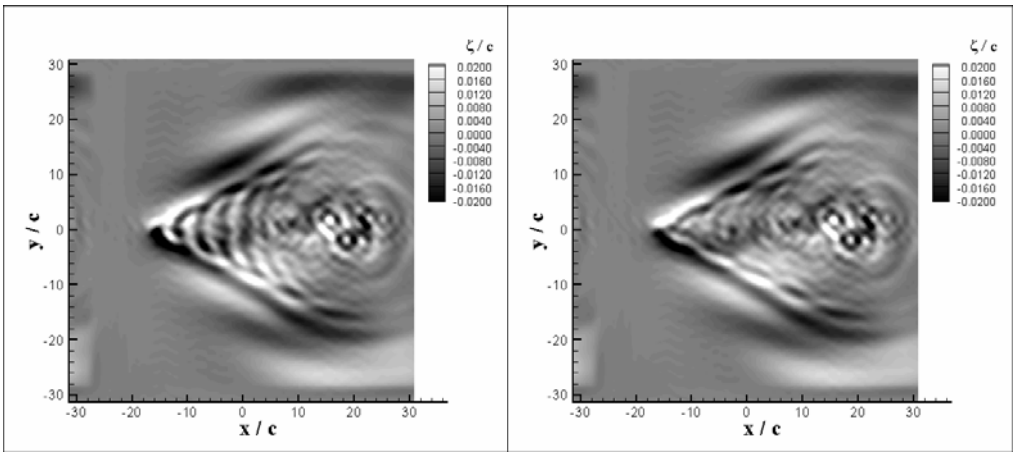

(c)

Fig. 4. Free-surface waves generated by the heaving motion of a vertical foil with $s/c = 5, F_r = 0.80, d/c = 0.5$, and $h/c = 0.25$ at (a) $\tau = 0.10$, (b) $\tau = 0.25$, and (c) $\tau = 0.50$. The wave fields shown are with (left) or without (right) steady Kelvin wake components. The submergence *h* is defined to be the distance from the mean free surface to the top end of the foil.

4.3 Free-surface signature of a moored underwater buoy

We consider the nonlinear interaction problem of surface waves with a tethered near-surface buoy, as shown in Fig. 5. Unlike most previous studies on the subject of the dynamics of tethered objects in waves which have been limited to the prediction of hydrodynamic loads on the structures and mooring systems, in the present study, our main interests are the mechanisms of generating short free-surface waves by the motion of moored near-surface objects which may be detectable by remote sensing. Our objective is to investigate mechanisms for nonlinear short surface wave generation in this complete coupled wave-buoy-cable dynamical system. The detailed investigation of this problem can be found in Zhu *et al* (1999).

Systematic simulations show that beyond a small threshold value in the incident wave amplitude, the buoy performs chaotic motions, characterized by the snapping of the cable. The root mechanism of the chaotic response is the interplay between the nonlinear dynamics of the cable and the generation of surface waves, which provides a source of strong (radiation) damping. As a result of this interaction, the chaotic buoy motion switches between two competing modes of snapping response: one with larger average peak amplitude and lower characteristic frequency, and the other with smaller amplitude and higher frequency (see Fig. 6). The generated high-harmonic/short surface waves are greatly amplified once the chaotic motion sets in (Fig. 7), owing to the fact that the chaotic motion has a

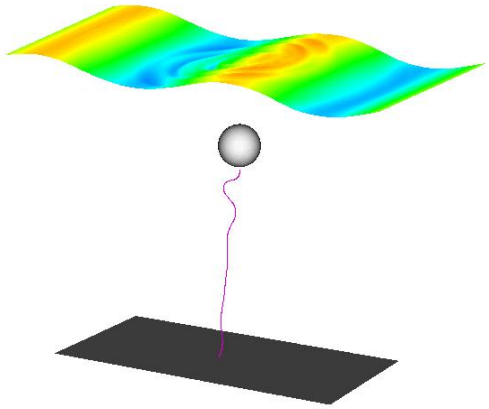

Fig.5. Sketch of a moored underwater buoy in waves.

broadband spectrum with significant amount of energy spread to high-frequency motions.

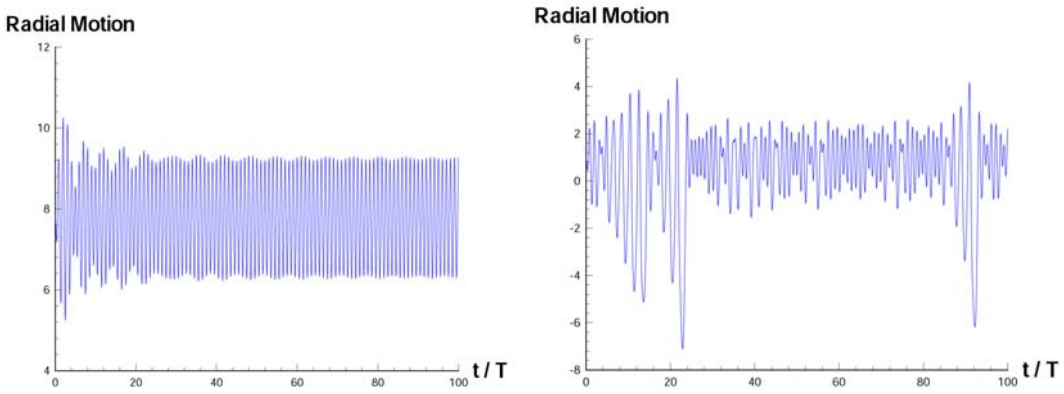

(a) (b)

Fig. 6. Response of the buoy to (a) small incident waves; (b) large incident waves.

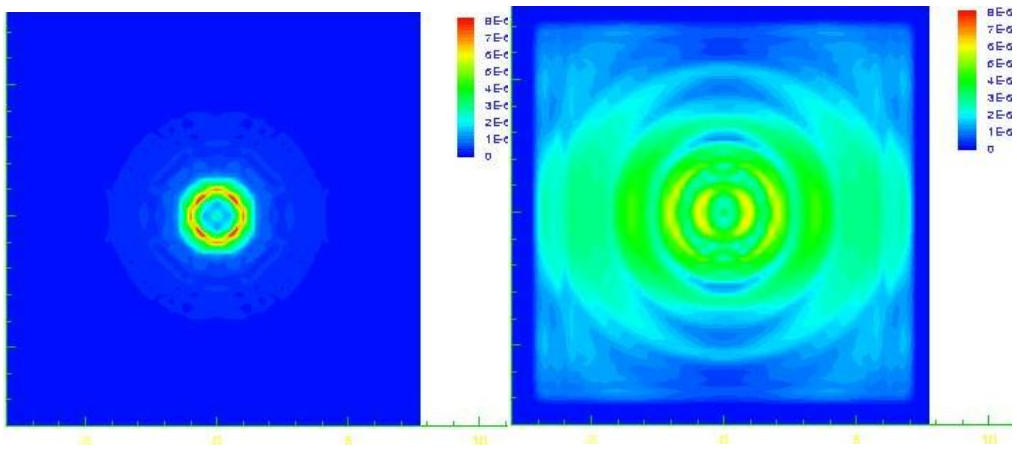

(a) (b)

Fig.7. Spectral of the generated free-surface disturbances for the cases of (a) small incident wave; and (b) large incident wave.

5. Conclusions

We apply two related effective numerical algorithms, the high-order spectral (HOS) method and the hybrid method to illustrate the distinctive free-surface wave patterns generated by various underwater objects. For a spheroid in forward motion, the HOS method provides high-resolution description of the combined wave field. For a submerged foil undergoing forward motion and oscillation, our numerical model demonstrates a combined wave field of steady Kelvin waves, unsteady waves, and vorticity-generated waves. For a moored underwater buoy, our numerical investigation shows the occurrence of chaotic motion, and the corresponding amplified short wave generation which may be detectable via remote sensing.

References

Dommermuth, D.G., Yue, D.K.P., 1987. A high-order spectral method for the study of nonlinear gravity waves. *J. Fluid Mech*. **184**, 267-288.

Liu, Y., Dommermuth, D.G., Yue, D.K.P., 1992. A high-order spectral method for nonlinear wave-body interactions. *J. Fluid Mech*. **245**, 115-136.

Mei, C.C. & Naciri, M. Note on ship oscillations and wake solitons. *Proc. R. Soc. Lond*., A**432**: 535-546, 1991.

Newman, J.N., 1992. The Green function for potential flow in a rectangular channel. *J. Enging. Math*. **26**, 51-59.

Tjavaras,A.A., Zhu,Q., Liu,Y., Triantafyllou,M.S. & Yue,D.K.P. The mechanics of highly-extensible cables. *J. Sound and Vibration.* **213**(4):709-737, 1998.

Zakharov, V.E. Stability of periodic waves of finite amplitude on the surface of a deep fluid. *J. Appl. Mech. And Tech. Phys*. **9**: 190-194 (English Trans.), 1968

Zhu, Q. Features of nonlinear wave-wave and wave-body interactions. Ph.D thesis. Massachusetts Institute Techonlogy, Cambridge, MA.

Zhu,Q., liu,Y., Tjavaras,A.A., Triantafyllou,M.S. & Yue,D.K.P. Mechanics of nonlinear short-wave generation by a moored near-surface buoy. *J. Fluid Mech.* **381**, 305-335, 1999.

Zhu, Q., Liu, Y. & Yue, D.K.P. Three-dimensional instabilities of standing waves. *J. Fluid Mech.* **496**, 213-242, 2003.

Zhu, Q., Liu, Y. & Yue, D.K.P. 2006. Dynamics of a three-dimensional oscillating foil near the free surface. *AIAA J*. In press.

Zhu, Q., Wolfgang, M., Yue, D.K.P., Triantafyllou, M.S., 2002. Three-dimensional flow structures and vorticity control in fish-like swimming. *J. Fluid Mech.* **468**, 1-28.